An Enhanced Fusion Algorithm With Empirical Thermoelectric Models for Sensorless Temperature Estimation of Li-ion Battery Cells

Mahroo Sajid, Ala A. Hussein, *Senior Member, IEEE*, Ali Wadi, *Member, IEEE*, and Mamoun F. Abdel-Hafez, *Senior Member, IEEE*

***Abstract*—An enhanced dual extended Kalman filter method is presented in this article for estimating and tracking the state-of-temperature of lithium-ion battery cells. A simple but effective dynamic and measurement empirical fit models are proposed and utilized to estimate the state-of-temperature concurrently with the state-of-charge. The proposed dual estimator improves the estimation accuracy of the temperature state by accounting for the variations in the state-of-charge. To test the performance of the proposed estimation method, two independent lithium-ion battery cell datasets were used to derive the empirical models and run the estimation algorithm. The obtained results show a promising performance of the estimation method in terms of the high estimation accuracy even in the case when the measurement contains high-magnitude noise or when the estimation algorithm is inaccurately initialized. The proposed models and the estimation algorithm are derived and experimentally tested in this article.**

***Index Terms*—Battery cell, dual estimation, extended Kalman filter, lithium-ion, state-of-charge, state-of-temperature.**

Nomenclature

BMS	Battery management system.
DEKF	Dual extended Kalman filter.
EKF	Extended Kalman filter.
EVs	Electric vehicles.
Li-ion	Lithium-ion.
MAE	Mean absolute error.
MLE	Maximum likelihood estimation.
OCV	Open-circuit voltage.
RMSE	Root mean square error.
SOC	State-of-charge.
SOH	State-of-health.
SOT	State-of-temperature.

Manuscript received 12 October 2022; revised 22 November 2022; accepted 25 December 2022. Date of publication 27 January 2023; date of current version 18 April 2023. Recommended by Technical Editor L. Wu and Senior Editor Z. Gao. An earlier version of this work was presented at the 2021 IEEE Energy Conversion Congress & Exposition (ECCE) Conference, Vancouver, BC, Canada, October 10–14, 2021 [DOI: 10.1109/ECCE47101.2021.9595866]. This work was supported by the Open Access Program from the American University of Sharjah. *(Corresponding author: Ala A. Hussein.)*

Mahroo Sajid, Ali Wadi, and Mamoun F. Abdel-Hafez are with the Department of Mechanical Engineering, American University of Sharjah, Sharjah 26666, UAE (e-mail: g00084312@aus.edu; awadi@aus.edu; mabdelhafez@aus.edu).

Ala A. Hussein is with the Department of Electrical Engineering, Prince Mohammad Bin Fahd University, Khobar 34754, Saudi Arabia (e-mail: ahussein@ieee.org).

Color versions of one or more figures in this article are available at https://doi.org/10.1109/TMECH.2023.3235726.

Digital Object Identifier 10.1109/TMECH.2023.3235726

I. Introduction

IN BATTERY products, in general, and in EVs specifically, implementing a reliable temperature monitoring mechanism is priceless as it plays a crucial role in preventing fire accidents, or in the best case scenario, premature end of service life [1], [2], [3]. Due to the produced heat by the Ohmic I^2R losses in a Li-ion battery cell, an increase in temperature occurs inside the battery and perhaps even thermal runaway. Thus, these batteries must be fully protected against overheat to avoid unwanted consequences such as fire hazard or premature end of life [4], [5], [6].

In this context, thermal sensors have been widely utilized in measuring the surface temperature of batteries due to their low cost. These sensors, however, must be calibrated frequently to be reasonably reliable, which is costly and possesses various challenges specifically in remote applications or when a massive number of sensors are employed to monitor the temperature of each cell in a battery pack. Moreover, temperature sensors are widely prone to failure due to internal self-heating, abuse or ageing, which cause irreversible change to the internal parameters and characteristics of the sensor that reduces its performance [7]. These potential sensor faults pause critical consequences when the sensors are deployed in sensitive applications such as those involving Li-ion batteries.

Hence, many sensorless temperature estimation methods have been proposed recently to estimate the temperature of Li-ion batteries. Many methods found in literature estimate the temperature from the impedance measurement where the impedance is computed by injecting an ac to the cell and recording the cell's voltage response. For example, in [8], the zero-crossing frequency, i.e., the frequency at which the internal impedance of the battery is purely resistive, was employed in a lookup table

that stores the corresponding temperature for each frequency. Due to its open-loop nature, the method in [8] will have a reduced accuracy if the zero-crossing frequency is inaccurate or not stored in the lookup table. A lookup table was used in [9] and [11] while a fit model was used in [10] to extract the temperature from the impedance measurement. A similar approach was adopted in [12] and [13]. The methods in [14] utilize a Kalman filter to estimate the temperature from the zero-crossing frequency measurement, and hence it adds more credibility to the temperature estimation mechanism. Kalman filters, however, assume the availability of noise statistics, which is not necessarily true in practice. According to these studies, the internal temperature of a battery cell is correlated with its internal impedance. Due to the need of using advanced hardware for impedance measurement, these methods are costly, in general, making them unsuitable for many applications.

To reduce the hardware requirements and the overall cost of the temperature estimation system, the surface (external) temperature is estimated instead of the internal temperature in small battery cells with negligible heat transfer delays. In [15], a recurrent neural network method is proposed for surface temperature estimation of Li-ion batteries of EVs. A feedforward network is proposed in [16] to estimate the surface temperature of lithium- and nickel-based batteries. A more advanced neural network is proposed in [17] where both the surface temperature and the SOC are estimated concurrently using a hybrid electrochemical-thermal model that accounts for the battery electrical and thermal dynamics. A deep-learning neural network method is proposed in [18] for surface temperature estimation of Li-ion batteries for electric vehicles. Other similar methods were proposed in [19] and [20]. As other data-driven methods, the referenced methods demand massive data to compute the weight functions of the neural network throughout training. Moreover, due to their open-loop nature, these models will fail, or in the best case scenario will have a declined performance, if the operating conditions are different than the training settings.

A method which employs an EKF algorithm that estimates the surface temperature accurately even when the initial temperature used is inaccurate or when the measurement contains high-magnitude noise is proposed in [21]. Although this method is relatively new and has shown promising results, the dependence of the temperature on the SOC was not investigated. In addition, EKF algorithms in general fail to provide accurate results if the noise covariance is unknown or in cases of biased measurement noise.

This article is an extension to the previously published work in [21]. An enhanced DEKF algorithm is proposed in this article to estimate the SOT and SOC, concurrently, by employing simple but effective thermo-electric fit models that correlate the voltage of the battery cell with its SOT and SOC. Although the SOC is estimated in this article, it is not the goal of this work. Instead, the motivation of this work is to develop an accurate estimation mechanism for the SOT that accounts for the dependency of the measurement model on the SOC by employing a DEKF estimation algorithm. In addition, the presented method accounts for the uncertainties in the measurement noise as it employs an MLE algorithm, [22], along with the traditional EKF. The enhancing MLE algorithm is used to identify the uncertainty statistics in a dynamic system. In the proposed method, the likelihood of the measurements is maximized with respect to the covariance matrices of the process and measurement noise sequences [23]. Once steady-state condition is reached, the measurements residual is formulated into a multivariate normal distribution vector with an associated covariance expressed in terms of the noise covariances [24], [25], [26], [27]. The approach identifies the covariance of the process and measurement noise, therefore allowing for compensating for any inaccuracy in the system model.

The proposed SOT estimation method has several merits compared with existing methods; namely, it demands low implementation cost as traditional sensor methods do, and it has a high performance as observer- and data-driven- methods do. The merits of the proposed method are as follows.

1) It has a low implementation cost as it avoids the tedious and costly impedance measurement utilized in [8], [9], [10], [11], [12], [13], and [14]. In addition, the proposed method demands no data resources contrary to neural network methods [15], [16], [17], [18], [19], [20].
2) It has a high accuracy due to its closed-loop nature, which is a powerful feature when operating under highly dynamic conditions that cannot be handled in the training phase of neural networks, [15] and [20]. Also, it is more accurate than traditional EKF methods, [21], since the proposed method does not assume fixed level/knowledge of the measurement and process noise statistics.

The outline of this article is as follows. Section II illustrates the thermal and heat transfer dynamics in batteries. Section III provides an introduction to the dataset used for models' derivation and experimental verification. Section IV presents the dynamic and measurement model employed in the proposed estimation algorithm. The estimation algorithm and its enhanced version are derived in Sections V and VI, respectively. Experimental verification and discussion are provided in Section VII. Finally, conclusions are drawn in Section VIII.

II. Thermal Dynamics and Heat Transfer Modeling

The thermal dynamics of a battery involve sophisticated electrochemical processes. These dynamics are impacted by several environmental and operational factors such as the ambient temperature, which directly impacts the surface temperature of the battery. The magnitude of the current going in/out the battery is another factor that contributes to the surface temperature as the internal losses in the battery, i.e., Ohmic I^2R losses, are proportional to the internal heat generation inside the battery. The heat generated inside the battery is also dependent on the battery age or SOH; as the battery ages, its internal resistance rises resulting in more temperature rise.

The thermal and heat transfer dynamics in a battery cell can be described using the equivalent-circuit models in Fig. 1 [32], where in Fig. 1(a), the OCV is the open-circuit voltage of the cell, R_0 is the internal resistance. In Fig. 1(b), P_{loss} is the power losses inside the cell, T_{a} is the ambient temperature, T_{i} and T_{s} are the internal and surface temperatures, C_{i} and C_{s} are the internal

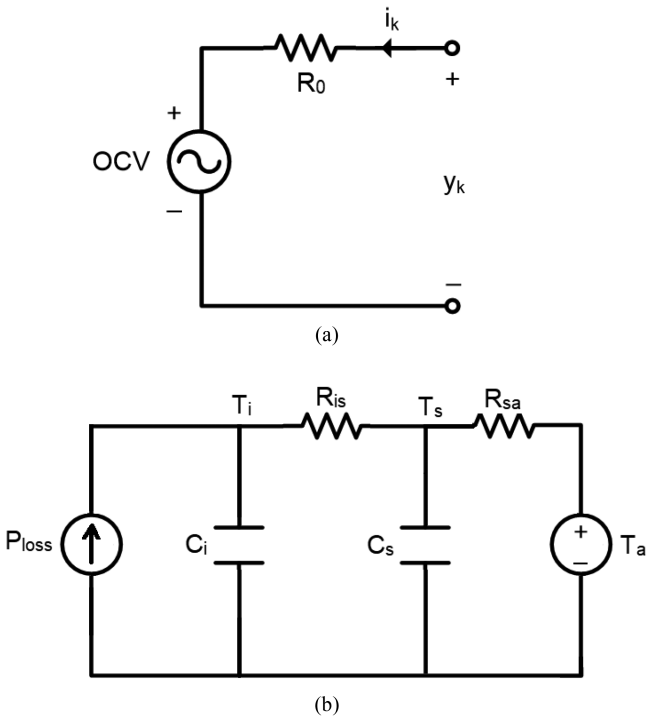

Fig. 1. (a) Electrical equivalent-circuit model. (b) Thermal equivalent-circuit model.

and surface heat capacity, $R_{\rm is}$ and $R_{\rm sa}$ are the internal-to-surface and surface-to-ambient thermal resistances of the cell [32].

Equation (1) represents the internal power loss, $P_{\rm loss}$, in the battery cell. The thermal dynamics based on the thermal model in Fig. 1(b) are expressed as in (2) and (3).

$$P_{loss} = R_0\, I^2 \tag{1}$$

$$C_i \frac{dT_i}{dt} = P_{loss} - \frac{T_i - T_s}{R_{is}} \tag{2}$$

$$C_s \frac{dT_s}{dt} = \frac{T_i - T_s}{R_{is}} - \frac{T_s - T_a}{R_{sa}} \tag{3}$$

Referring to Fig. 1(b), the power losses and the ambient temperature are modeled as external inputs to the model that directly impacts the battery temperature. If the battery had been in rest mode for a long time (∼several hours), both its internal and surface temperatures will be equal to the ambient temperature. When the battery is under charge or discharge, the power losses will cause the temperature to rise due to the internally generated heat, where this heat will transfer from the core to the surface of the battery at a rate that depends on the thermal resistances and capacitances of the battery. For a battery with a small physical size, the internal-to-surface thermal resistance will be small and the difference between the internal and surface temperature can be neglected.

One remark here is that the internal temperature is more correlated with the internal heat generation than the surface temperature. Hence, for fault detection and diagnostics, the internal temperature would be more accurate than the surface temperature. During normal operation and assuming a healthy battery cell, the surface temperature should provide sufficient information to the BMS to manage the charge going in/out the cell. In the rest of this article, the "temperature" will always refer to the surface temperature of a brand-new healthy battery cell.

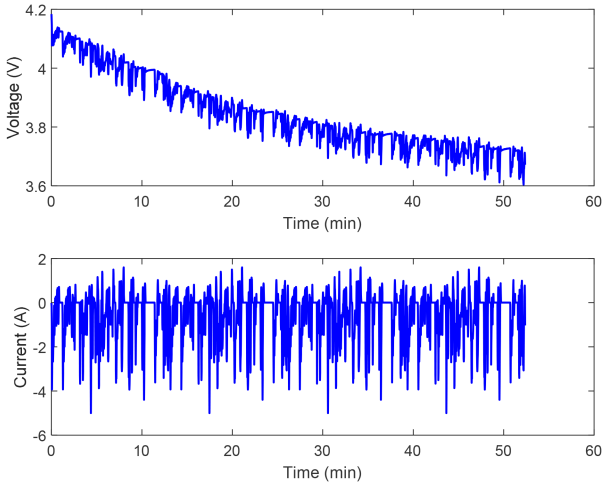

Fig. 2. Voltage and current of the Oxford dataset.

III. Battery Cell Datasets

In this section, two public Li-ion battery cell datasets are presented. These datasets are used later to derive the proposed dynamic models and for experimental verification of the proposed method.

A. Oxford Dataset

The first dataset used in this article is the "Oxford Battery Degradation Dataset 1" which contains battery ageing data measured at 40 °C ambient temperature from eight small Li-ion battery pouch cells [28]. The charge cycle follows a constant-current, constant-voltage charge profile which is followed by a discharge profile based on the urban Artemis driving cycle. In this article, the voltage, current, and temperature data of the first discharge cycle are considered for modeling purposes. Figs. 2 and 3 show the data of this cycle. The temperature is replotted in Fig. 4 after applying a low-pass filter to the data to reduce the fluctuating noise.

B. NASA Dataset

The second dataset used is obtained from NASA's Prognostics Data Repository [29]. Three different operational profiles, namely, charge, discharge, and impedance, were run on a set of four Li-ion battery cells (5, 6, 7, and 18) at room temperature, i.e., 24 °C. In this article, the discharge data (voltage, current, and temperature) for cell 5 are used for a SOH range from 100% (new condition) to 70%, which corresponds to a capacity fade from 2 to 1.4 Ah (30% capacity fade).

In this dataset, a constant 2 A discharge current is used until the voltage drops to 2.7 V. Repeated charge and discharge cycles were used to accelerate the ageing process of the cell until the

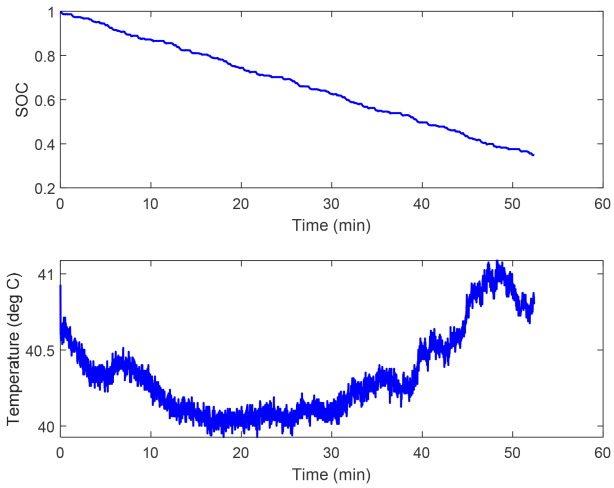

Fig. 3. SOC and temperature of the Oxford dataset.

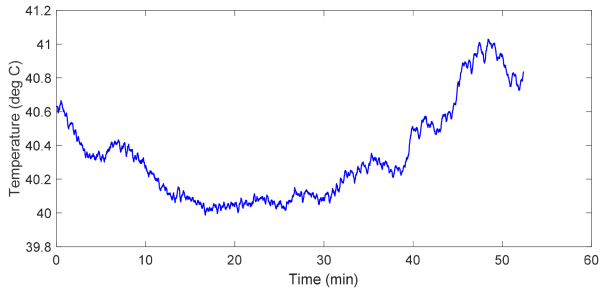

Fig. 4. Filtered temperature of the Oxford dataset.

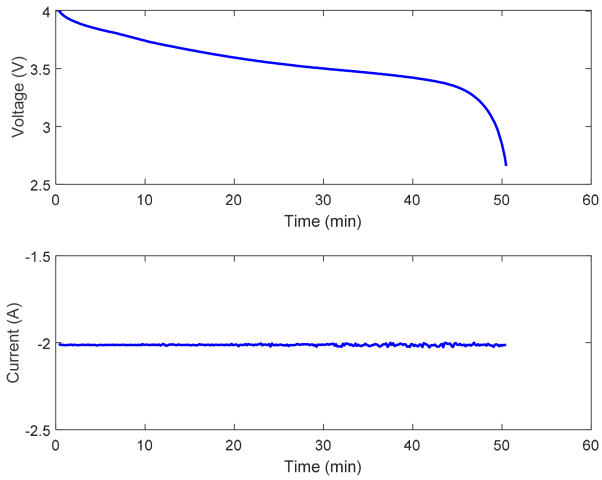

Fig. 5. Voltage and current of the NASA dataset (cycle 200).

30% capacity fade is achieved. Fig. 5 shows the voltage and current profile for cycle 200, which is a discharge cycle. Fig. 6 shows the variation in SOC and temperature for the same cycle. The voltage, current, and temperature profiles are smooth as compared with the first dataset where a lot of fluctuations could be observed, which is due to the constant current used in this

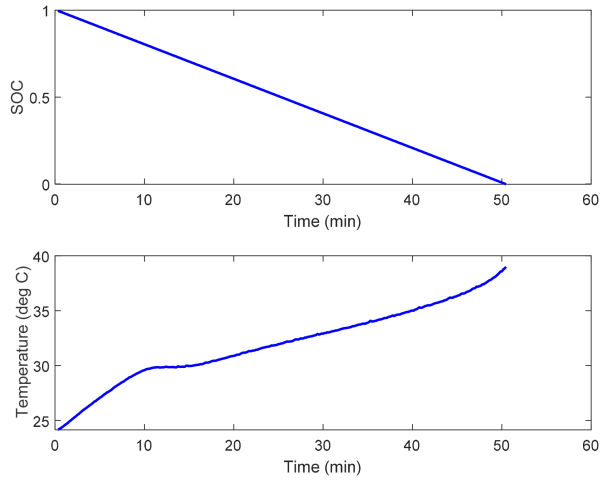

Fig. 6. SOC and temperature of the NASA dataset (cycle 200).

dataset and perhaps the lower noise level compared with the first dataset.

IV. Dynamic and Measurement Models

The dynamic and measurement models utilized by the proposed estimation algorithm are detailed in this section.

A. Models for SOT Estimation

The SOT can be mathematically derived using the electrothermal model in Fig. 1(b). This model, however, is quite sophisticated and demands frequent offline tuning to ensure accurate temperature estimation. Instead, we are proposing two dynamic models and another two measurement models based on curve fitting approach to be used for SOT estimation. Equation (4) shows the first discretized system model derived for the Oxford dataset in the general form while (5) represents the equation of the closest fit:

$$T_{k+1} = f_1\ (T_k, I_k) + w_k \tag{4}$$

$$T_{k+1} = T_k\ + 8.65 * 10^{-4}(\mathrm{I_k})^2 + w_k. \tag{5}$$

In (4) and (5), T_k is the cell's surface temperature, I_k is the current, w_k is the process noise, and k is a time index. The function f_1 was found experimentally by curve fitting. The model is obtained using the temperature and current from the first discharge cycle.

The discretized measurement model is given in the following equation:

$$V_k = f_2\ (T_k,\ SOC_k, I_k) + v_k \tag{6}$$

where V_k is the voltage, T_k is the temperature, ν_k is the measurement noise, f_2 is a function determined by curve fitting, and k is the time index.

Several higher-order measurement models were tested to obtain an accurate measurement function, f_2. However, a linear model was found to have the best R square (goodness of fit measure) of 0.998. The discrete-time measurement model for the

system was found through regression resulting in the following model:

$$V_k = 0.08424\, T_k + 0.6869\, SOC_k + 0.0203\, I_k + v_k. \quad (7)$$

Polynomial models for the system and measurement equations, similar to those given in (4)–(7), were derived for the NASA dataset and are given in the following equations:

$$T_{k+1} = 0.9981 T_k + 0.3736(\mathrm{I}_k)^2 - 1.407 + w_k \quad (8)$$

$$\begin{aligned} V_k = & -2.181\, T_k + 0.0243(T_k)^2 - 8.97\, SOC_k \\ & + 7.7712\, (SOC_k)^2 + 0.9404\, T_k\, SOC_k \\ & + 0.1155\, I_k + 51.1947 + v_k. \end{aligned} \quad (9)$$

The polynomial models described earlier give sufficiently good results in the case of the Oxford dataset, which is highly dynamic. However, for the NASA dataset, polynomial models do not result in optimal temperature estimates. Therefore, the system model was derived again with a polynomial model for the system dynamics and a Gaussian model for the measurement equation. The Gaussian model involves exponential terms which suits the shape of the voltage curve (as shown in Fig. 5).

$$\begin{aligned} T_{k+1} = & \ 0.7993 T_k + 0.00312\, (T_k)^2 + 0.05315(\mathrm{I}_k)^2 \\ & - 0.0003826\, T_k (I_k)^2 - 3.031 + w_k \end{aligned} \quad (10)$$

$$\begin{aligned} V\ (k) = & \ 3.923\, e^{\left(\frac{-(T(k)-T_a-0.59)}{20.6}\right)^2} \\ & + 0.5148\, e^{\left(\frac{-(T(k)-T_a-12.84)}{3.641}\right)^2} + v\,(k)\,. \end{aligned} \quad (11)$$

It shall be noted that the coefficient of the derived models can be adjusted online or offline to account for the cell-to-cell variations if they are run on different battery cells.

B. Models for SOC Estimation

In an experimental setting, the true SOC is not available, and hence it must be estimated alongside the SOT. Not only is it a quantity of interest, but also it is used in the proposed polynomial model in modeling the SOT. The SOC dynamic and measurement models are visually presented in Fig. 1(a) and mathematically expressed in (12) and (13), respectively.

$$SOC_{k+1} = SOC_k + \eta \frac{\Delta t}{C_n} i_k + w_k \quad (12)$$

$$y_{k+1} = OCV\,(SOC_{k+1}) + R_0\, i_k + v_{k+1} \quad (13)$$

where SOC_k is the state-of-charge at time step k, Δt is the sampling time, η is the dis/charge efficiency (assumed 100% for a brand new Li-ion battery cell), C_n is the nominal capacity of the battery in Ampere-second, OCV is the open-circuit voltage (also known as electromotive force), R_0 is the internal resistance of the cell that accounts for the internal voltage drop and heat generation, i_k is the current at time step k, w_k is the added process noise, y_{k+1} is the model's voltage at $k+1$, and v_{k+1} is the measurement noise. The current i_k is considered negative during discharging and positive during charging. One remark here is that both w_k and v_{k+1} are assumed independent and identically distributed white noise sequences of zero mean and Q and R covariances, respectively.

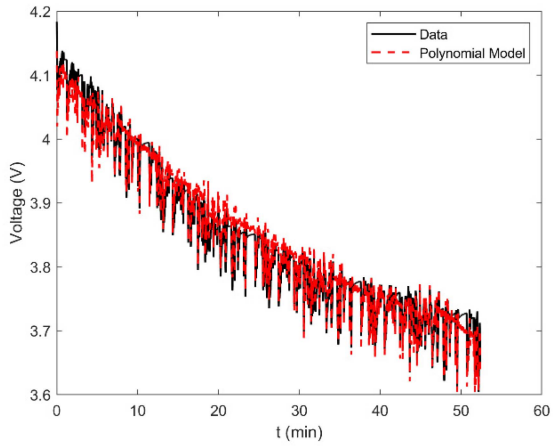

Fig. 7. Polynomial measurement model versus true voltage for the Oxford dataset.

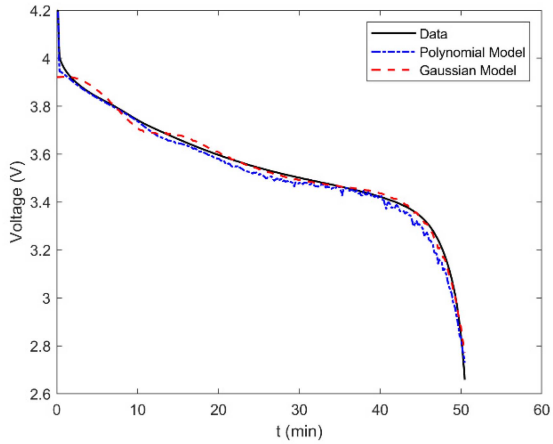

Fig. 8. Polynomial and exponential measurement models versus true voltage for the NASA dataset.

TABLE I
RMSE FOR PROPOSED MODELS

	Oxford dataset	NASA dataset
Polynomial model	0.0017 V	0.0204 V
Gaussian model	N/A	0.0013 V

C. Evaluation of Proposed Models

The presented models, i.e., polynomial and Gaussian (exponential) models, are plotted against the true voltage measurement for the two datasets. According to Figs. 7 and 8, the two models have almost the same level of accuracy. The exponential model, however, has a slightly higher accuracy in the constant-current discharge test, i.e., NASA dataset, as it is more capable to capture the exponential decay in the voltage as the battery approaches 0% SOC. The RMSE of these models is given in Table I.

V. Estimation Algorithm

Since the battery is a nonlinear system, a nonlinear observer must be used to estimate its temperature state. Among many alternatives, EKF is an excellent selection as EKFs are well-established with proven capability in estimating nonlinear systems states [27]. First, the nonlinear system equation needs to be linearized. Assuming the SOC is known, the Jacobians of the dynamic and measurement equations are given as follows:

$$F_k = \frac{\partial f_1}{\partial T} \tag{14}$$

$$H_k = \frac{\partial f_2}{\partial T}\,. \tag{15}$$

These Jacobians are evaluated about the most recent estimate of the temperature to find the filter gain K_{k+1}, the innovation covariance S_{k+1} and the state prediction covariance $P_{k+1|k}$. Hence, the following updated state estimate is obtained:

$$\hat{T}_{k+1|k+1} = \hat{T}_{k+1|k} + K_{k+1}\,\upsilon_{k+1} \tag{16}$$

where υ_{k+1} is the measurement residual given as follows:

$$\upsilon_{k+1} = V_{k+1} - \hat{V}_{k+1|k}. \tag{17}$$

The predicted state $\hat{T}_{k+1|k+1}$ is the function f_1 evaluated at the previous estimate $\hat{T}_{k|k}$ and measurement prediction $\hat{V}_{k+1|k}$ is the function f_2 evaluated at the state prediction $\hat{T}_{k+1|k}$.

To estimate the SOT and SOC concurrently, a dual filter scheme that aims to sequentially estimate these states is proposed. The dual estimation approach is especially useful as it reduced the dimensionality of the joint SOC-SOT estimation problem, where the two states would form one higher dimension state vector. Therefore, the computational requirement of the algorithm is reduced. The dual algorithm starts by initializing the SOC and SOT states and their respective initial covariances with $\hat{x}_1 \leftarrow x_0$, $\hat{\boldsymbol{P}}_1^x \leftarrow \mathrm{P}_{x_0}$ and $\hat{T}_1 \leftarrow T_0$, $\hat{\boldsymbol{P}}_1^T \leftarrow \mathrm{P}_{T_0}$, respectively, where $\bar{x}_k$ is the *a priori* estimate of the SOC at time k given measurements up to time $k-1$, whereas $\hat{x}_k$ is the *a posteriori* estimate of the SOC given measurements up to time k. Likewise, this notation applies to T_k and P_k.

The state filter is then propagated through time using the EKF equations as follows:

$$\bar{x}_{k+1} = \hat{x}_k + (\eta \Delta t / C_n)\, i_k \tag{18}$$

$$\bar{\mathbf{P}}_{x,k+1} = \hat{\mathbf{P}}_{x,k} + \mathrm{Q}_{w,k} \tag{19}$$

$$\mathrm{H}_k^x = \left.\frac{\partial h\,(x_k,\, i_k)}{\partial x}\right|_{x\,=\bar{x}_k} = \frac{(z_k\,(\bar{x}_k) - z_{k-1}\,(\bar{x}_{k-1})\,)}{\bar{x}_k - \bar{x}_{k-1}} \tag{20}$$

$$\mathrm{K}_k^x = \bar{\mathbf{P}}_{x,k}\,(\mathrm{H}_k^x)^T \left[\boldsymbol{H}_k^x\,\bar{\boldsymbol{P}}_{x,k}(\boldsymbol{H}_k^x)^T + \boldsymbol{R}_{v,k}\right]^{-1} \tag{21}$$

where (18) is the dynamic model in Section IV-B, and is the measurement model in the same section, i.e., $h\,(x_k,\, i_k) = OCV(x_k) + i_k R_0$.

Similarly, the SOT estimator is propagated through time using the following equations:

$$\bar{T}_{k+1} = f_1\,\left(\bar{x}_k,\, i_k, \hat{T}_k\right) \tag{22}$$

$$F_k = \left.\frac{\partial f_1\,(\bar{x}_k,\, i_k, T_k)}{\partial T}\right|_{T_k=\hat{T}_k} \tag{23}$$

$$\bar{\mathbf{P}}_{T,k+1} = F_k \hat{\mathbf{P}}_{T,k} F_k^{\mathrm{T}} + \mathrm{Q}_{r,k} \tag{24}$$

$$\mathrm{H}_k^\theta = \left.\frac{\partial f_2\left(\bar{x}_k,\, i_k, \hat{T}_k\right)}{\partial T}\right|_{T_k=\bar{T}_k} \tag{25}$$

$$\mathrm{K}_k^\theta = \bar{\mathbf{P}}_{\theta,k}\,(\mathrm{H}_k^\theta)^T \left[\boldsymbol{H}_k^\theta\,\bar{\boldsymbol{P}}_{\theta,k}(\boldsymbol{H}_k^\theta)^T + \boldsymbol{R}_{e,k}\right]^{-1} \tag{26}$$

where f_1 and f_2 are the SOT process and measurement models proposed in Section IV-A.

Finally, the state filter is updated as follows:

$$\hat{x}_k = \bar{x}_k + \mathrm{K}_k^x\,\left(V_k - h\left(\bar{x}_k,\, i_k, \bar{T}_k\right)\right) \tag{27}$$

$$\hat{\mathbf{P}}_{x,k} = (I - \mathrm{K}_k^x \mathrm{H}_k^x)\,\bar{\mathbf{P}}_{x,k} \tag{28}$$

$$\hat{T}_k = \bar{T}_k + \mathrm{K}_k^T\,\left(V_k - h\left(\hat{x}_k,\, i_k, \bar{T}_k\right)\right) \tag{29}$$

$$\hat{\mathbf{P}}_{T,k} = \left(I - \mathrm{K}_k^T \mathrm{H}_k^T\right)\bar{\mathbf{P}}_{T,k} \tag{30}$$

where all the quantities have already been defined.

VI. Enhancement of Estimation Algorithm

The estimation algorithm in Section V assumes the availability of the process and measurements noise statistics represented by noise covariance magnitudes of the two filters. This is generally inaccurate as the noise statistics may not be perfectly known or can change because of sensors' aging, battery environment, and other factors that may introduce uncertainties. Thus, an adaptation method for the noise covariance magnitudes of the process and measurement processes is proposed. An MLE algorithm, [22], has been implemented in conjunction with the EKF algorithm to improve the accuracy of the temperature estimation by recursively estimating the process noise covariance matrix Q and measurement noise covariance matrix R.

The measurement innovation covariance S can be written in an alternative form as follows:

$$C_k = \sum_{j\,=\,k-N+1}^{k} \upsilon_{k+1}\upsilon'_{k+1} \tag{31}$$

where υ_{k+1} is the measurement residual defined in (17). C_k is statistically estimated over a moving window of size N. The updated estimate of Q is given as follows:

$$Q_k = K_k\,C_k K'_k. \tag{32}$$

Similarly, the measurement error covariance R_k is recursively updated as follows:

$$R_k = C_k - H_k P_{k|k-1} H'_k. \tag{33}$$

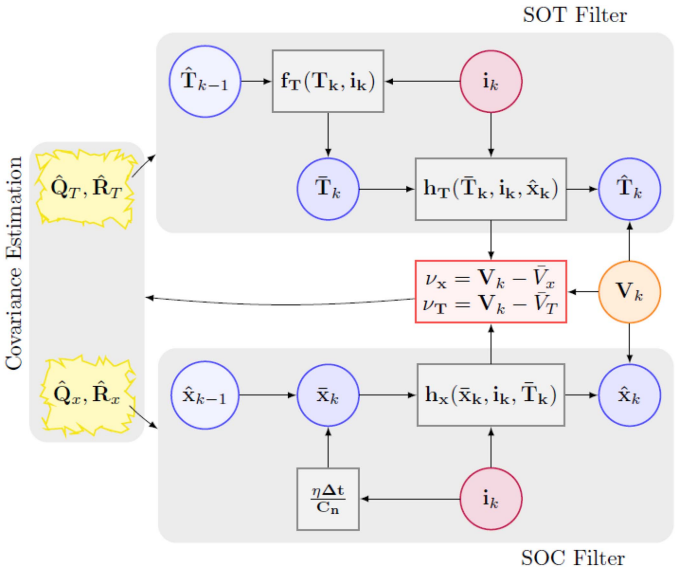

Fig. 9. Demonstration of the proposed dual EKF-with-MLE SOC/SOT estimator.

The final updated values of Q_k and R_k are obtained by the forgetting factor formula:

$$\hat{Q}_k = b_1 \hat{Q}_k + (1 - b_1)\, \hat{Q}_{k-1} \tag{34}$$

$$\hat{R}_k = b_2\, \hat{R}_k + (1 - b_2)\, \hat{R}_{k-1} \tag{35}$$

where $b_1, b_2 \in (0,\ 1)$ influence the memory span of the forgetting factor with higher values mean that more recent information plays a bigger role in the estimation. A demonstration of the proposed estimator is shown in Fig. 9.

To demonstrate the stability of the proposed filtering approach, the observability of the system is examined. In [30] and [31], the observability of multiple dynamic systems was investigated under different conditions. The observability is studied by inspecting the rank of the following constructed observability Gramian [30]:

$$O\ (t) = \begin{bmatrix} N_0\,(t) \\ N_1\,(t) \\ \vdots \\ N_{n-1}\,(t) \end{bmatrix} \tag{36}$$

where $N_0\,(t) = H(t)$, and $N_{k+1}\,(t) = F(t)N_k(t) + \frac{d}{dt}N_k(t)$, $k \in [\ 0 \quad n-1\ ]$.

The observability of the proposed algorithm was analyzed for the two proposed modeling approaches. $H(t)$ is computed by obtaining the partial derivative of (7) or (11) with respect to the temperature state, and $F(t)$ is computed by taking the partial derivative of (5) or (10) with respect to the temperature state. In both cases, the dynamic system of size $n = 1$ is shown to be observable, for the observability Gramian has full rank.

VII. Experimental Verification

The datasets in [28] and [29] were used to test the proposed estimation technique experimentally. The actual SOC values

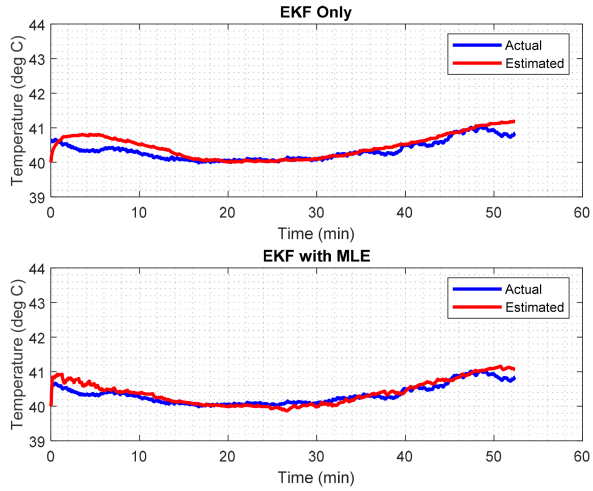

Fig. 10. Comparison of temperature estimation between EKF-only and EKF- with-MLE (Oxford dataset).

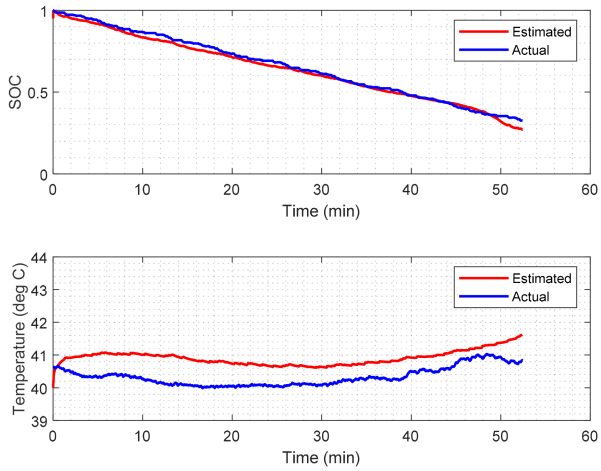

Fig. 11. Dual EKF-only SOC and SOT estimation results (Oxford dataset).

computed using coulomb-counting were used in order to estimate the temperature values in both datasets.

Temperature estimation results for the Oxford dataset obtained using the EKF and the MLE-aided EKF is shown in Fig. 10 when assuming the knowledge of the SOC. In these results, the polynomial model was used. With EKF alone, the MAE and RMSE values are 0.1394 °C and 0.1919 °C, respectively. When adapting the MLE algorithm, the MAE and RMSE error values are reduced to 0.1133 °C and 0.1475 °C, respectively.

Figs. 11 and 12 show the results of the dual SOC-SOT filter using the EKF and the MLE-aided EKF, respectively. In these results, rather than using the true SOC values, the SOC is first estimated, and the temperature is subsequently estimated based on the SOC estimate. The addition of the MLE algorithm resulted in reducing the temperature estimation error. The recorded MAE and RMSE values without the MLE algorithm are 0.5767 °C and 0.6008 °C, respectively, while these values go down to 0.2477 °C and 0.3158 °C when the MLE algorithm is implemented.

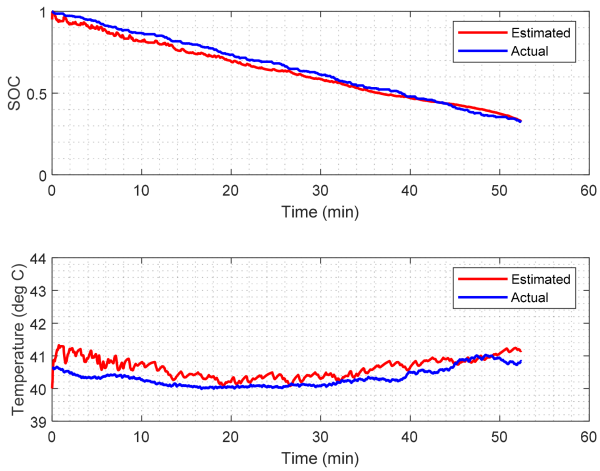

Fig. 12. Dual EKF-with-MLE SOC and SOT estimation results (Oxford dataset).

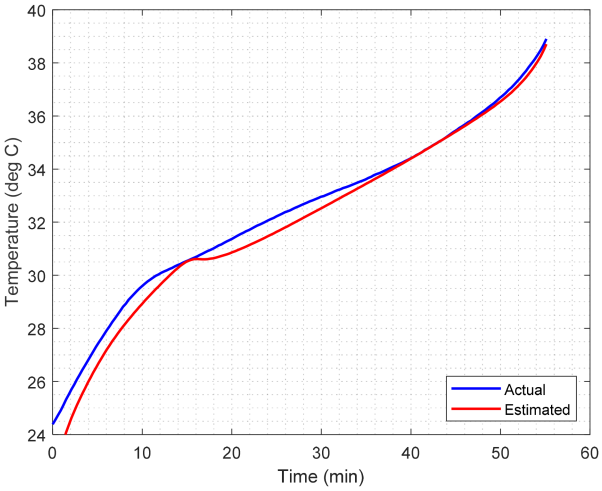

Fig. 13. Temperature estimation results using EKF-with-MLE and polynomial models (NASA dataset cycle 1).

The temperature estimation results for the NASA dataset using the polynomial models and the MLE-aided EKF algorithm are displayed in Figs. 13 and 14 for cycles 1 and 200, respectively. The RMSE value for cycle 1 is 0.6090 °C, while for cycle 200 it is 0.3880 °C. In Figs. 13 and 14, the true SOC values were used. As expected, when the dual estimation algorithm was implemented, the errors went up, in comparison with the case when the true SOC was used. This is due to the error in the SOC estimates. The estimation results for the dual MLE-aided EKF algorithm are shown in Figs. 15 and 16. The RMSE for the temperature estimates for cycles 1 and 200 are 1.3964 °C and 1.015 °C, respectively. The results in Fig. 15 were duplicated using the SOC-independent Gaussian measurement model (Figs. 17 and 18).

The obtained results for the NASA dataset utilizing the Gaussian model show an improvement in the temperature estimation accuracy with RMSE values of 0.3908 °C and 0.3722 °C for

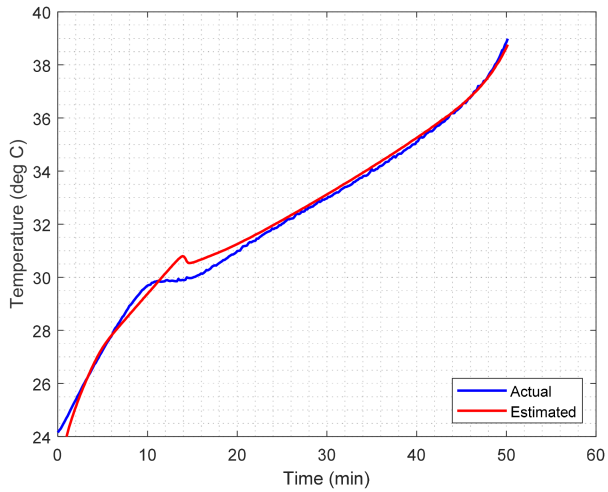

Fig. 14. Temperature estimation results using EKF-with-MLE and polynomial models (NASA dataset cycle 200).

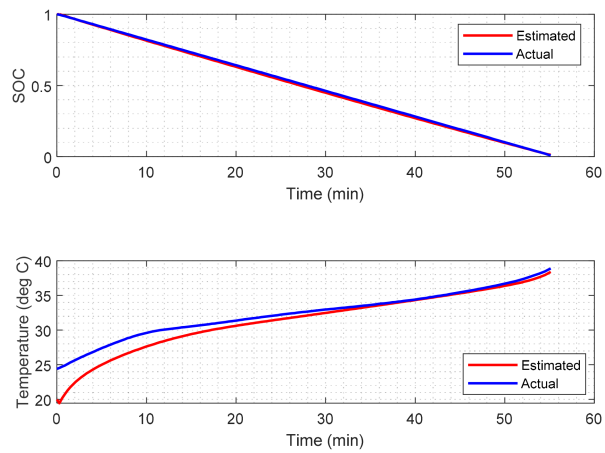

Fig. 15. Dual EKF-with-MLE SOC and SOT estimation results (NASA dataset cycle 1).

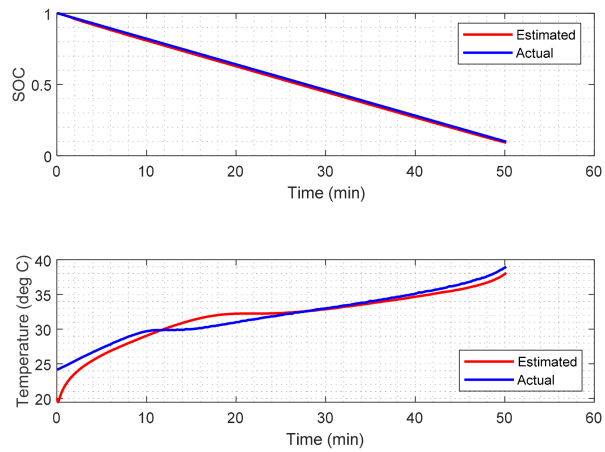

Fig. 16. Dual EKF-with-MLE SOC and SOT estimation results (NASA dataset cycle 200).

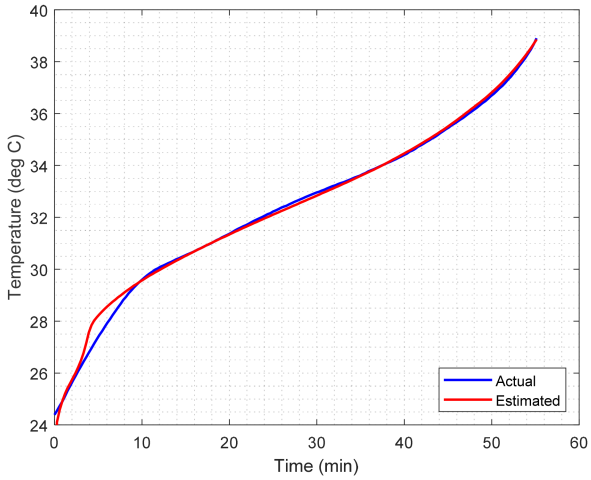

Fig. 17. Temperature estimation results using EKF-with-MLE and Gaussian measurement model (NASA dataset cycle 1).

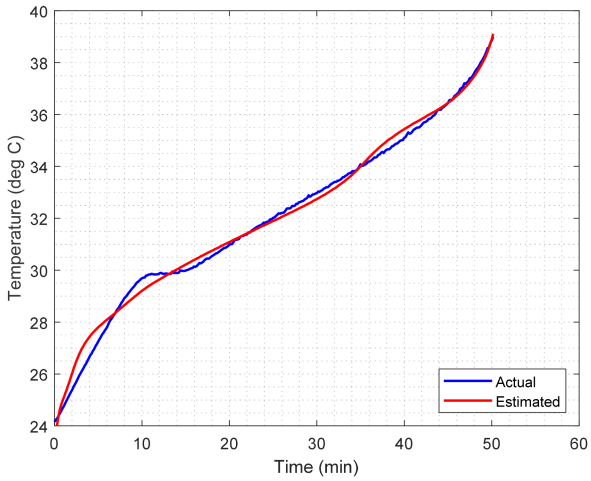

Fig. 18. Temperature estimation results using EKF-with-MLE and Gaussian measurement model (NASA dataset cycle 200).

cycles 1 and 200, respectively, compared with 1.3964 °C and 1.015 °C (cycles 1 and 200) when the polynomial fit model is used.

For further verification, an additional test was conducted using a 3.6 V, 1.1 Ah Li-ion battery cell. The cell was charged using a 1-A current to 3.6-V, then using a constant voltage of 3.6-V until the current dropped to 50-mA. The temperature estimation result using the proposed estimation algorithm and the polynomial model is shown in Fig. 19. In this figure, although the initial temperature was intentionally set at 20 °C, the algorithm was able to achieve convergence in less than 100 s with an RMSE of 0.3306 °C and MAE of 0.2546 °C. As can be noted in Fig. 19, the error suddenly increases at minute 55 (at the start of the constant-voltage mode) and peaks at minute 58 before it starts decreasing as the constant-voltage charging approaches its end when the battery approaches 100% SOC. This can be explained as when the charger switches from constant-current to constant-voltage mode, the measurement model tries to adapt

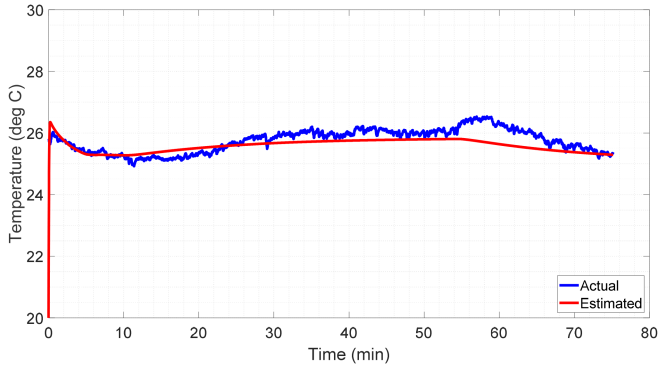

Fig. 19. Temperature estimation results using EKF-with-MLE and polynomial measurement model using a 3.6-V, 1.1 Ah Li-ion battery cell.

TABLE II
ESTIMATED TEMPERATURE RMSE FOR OXFORD DATASET (POLYNOMIAL MODEL)

Estimation Algorithm	RMSE
Traditional EKF	0.1919
Proposed EKF with MLE	0.1475

TABLE III
ESTIMATED TEMPERATURE RMSE FOR NASA DATASET (PROPOSED ALGORITHM)

Model	Cycle	RMSE
Polynomial model	1	1.3964
	200	1.015
Gaussian model	1	0.3908
	200	0.3722

to the new internal resistance value of the battery cell when the current starts dropping from 1000 to 50 mA throughout the constant-voltage charging mode. Another remark is that at the end of the constant-voltage mode, the internal voltage drop decreases due to the decreasing current when the battery approaches equilibrium and the temperature and the voltage settle, which explains why the error is less at the end of the constant-voltage mode. The error throughout the entire charging test did not exceed 0.8 °C. A summary of the obtained RMSE values of the estimated temperature using the conducted experiments is provided in Tables II and III.

According to the obtained results, the selection of the proper model for a specific dataset is crucial in improving the temperature estimation accuracy. In dynamic environments where the current going in/out the battery is highly dynamic, it was found that adding the SOT dependence on the SOC slightly improves the temperature estimation accuracy. This was achieved using the SOC-dependent polynomial measurement model and verified experimentally using the first dataset, i.e., Oxford dataset. On the other hand, when the current flowing in or out of the battery is almost constant, the SOC-independent Gaussian measurement model will provide much more accurate temperature estimation results as verified experimentally using the second dataset, i.e., NASA dataset. In this dataset, the reduction in RMSE was 72% for cycle 1 and 63% for cycle 200 when the

Gaussian model is used in comparison with the polynomial model.

To ensure accurate and reliable temperature estimation results, various models that accommodate different operating conditions must be implemented in the BMS. Moreover, besides adding an enhancing MLE algorithm along with the traditional EKF algorithm to improve the robustness of the estimation algorithm, an auto-tuning algorithm can be implemented to tune the model coefficients and allow the model to adapt to all possible operating conditions [33].

Lastly, although in many industrial applications and battery products a temperature sensor is thought to be sufficient to monitor the temperature of the battery, many Li-ion battery accidents related to thermal runaway are reported consistently. These add more concerns on the safety of the batteries. With advanced monitoring algorithms and a little additional cost, the safety and longevity of these batteries can be enhanced significantly, which with no doubt worth the added cost.

VIII. Conclusion

A sensorless surface temperature estimation method is proposed for Li-ion battery cells based on EKF approach. The estimation algorithm employs a DEKF to estimate the SOC and the SOT. Two measurement models were derived and implemented, namely, the polynomial and the Gaussian models. The proposed algorithm incorporates the dependence of temperature on the SOC. This was found to improve the temperature estimation accuracy in highly dynamic environments such as in EVs where the battery's current changes widely. Moreover, the proposed sensor fusion algorithm was augmented with an MLE-based noise covariance magnitudes identification routine to realize higher estimation accuracy by accounting for the possibly varying uncertainties in the implemented models as well as measurement sources available to the algorithm. In all conducted experiments, the proposed algorithm was able to converge, in a relatively short time, with a high accuracy.

Acknowledgment

This article represents the opinions of the author(s) and does not mean to represent the position or opinions of the American University of Sharjah.

References

[1] G. Xia, L. Cao, and G. Bi, "A review on battery thermal management in electric vehicle application," *J. Power Sources*, vol. 367, pp. 90–105, 2017.

[2] U.S. National Renewable Energy Laboratory (NREL), "Electric vehicle battery thermal issues and thermal management techniques," 2011. Accessed: Oct. 10, 2022. [Online]. Available: https://www.nrel.gov/docs/fy13osti/52818.pdf

[3] S. Dhameja, *Electric Vehicle Battery Systems*. Amsterdam, The Netherlands: Elsevier, 2001.

[4] L. Kong, C. Li, J. Jiang, and M. G. Pecht, "Li-ion battery fire hazards and safety strategies," *Energies*, vol. 11, no. 9, 2018, Art. no. 2191.

[5] D. H. Doughty and E. P. Roth, "A general discussion of Li ion battery safety," *Electrochem. Soc. Interface*, vol. 21, no. 2, pp. 37–42, 2012.

[6] L. H. J. Raijmakers, D. L. Danilov, R. A. Eichel, and P. H. L. Notten, "A review on various temperature-indication methods for Li-ion batteries," *Appl. Energy*, vol. 240, pp. 918–945, 2019.

[7] A. A. Hussein and A. A. Fardoun, "An effective impedance-phase method for sensorless measurement of Li-ion battery cells' internal temperature," in *Proc. IEEE Energy Convers. Congr. Expo.*, 2021, pp. 5899–5902.

[8] A. A. Hussein and A. A. Fardoun, "An adaptive sensorless measurement technique for internal temperature of Li-ion batteries using impedance phase spectroscopy," *IEEE Trans. Ind. Appl.*, vol. 56, no. 3, pp. 3043–3051, May/Jun. 2020.

[9] L. H. J. Raijmakers, D. L. Danilov, J. P. M. Van Lammeren, M. J. G. Lammers, and P. H. L. Notten, "Sensorless battery temperature measurements based on electrochemical impedance spectroscopy," *J. Power Sources*, vol. 247, pp. 539–544, 2014.

[10] R. R. Richardson, P. T. Ireland, and D. A. Howey, "Battery internal temperature estimation by combined impedance and surface temperature measurement," *J. Power Sources*, vol. 265, pp. 254–261, 2014.

[11] H. Beelen, L. H. J. Raijmakers, M. C. F. Donkers, P. H. L. Notten, and H. J. Bergveld, "A comparison and accuracy analysis of impedance-based temperature estimation methods for Li-ion batteries," *Appl. Energy*, vol. 175, pp. 128–140, 2016.

[12] X. Wang, X. Wei, Q. Chen, J. Zhu, and H. Dai, "Lithium-ion battery temperature on-line estimation based on fast impedance calculation," *J. Energy Storage*, vol. 26, 2019, Art. no. 100952.

[13] B. Liebhart, L. Komsiyska, and C. Endisch, "Passive impedance spectroscopy for monitoring lithium-ion battery cells during vehicle operation," *J. Power Sources*, vol. 449, 2020, Art. no. 227297.

[14] R. R. Richardson and D. A. Howey, "Sensorless battery internal temperature estimation using a Kalman filter with impedance measurement," *IEEE Trans. Sustain. Energy*, vol. 6, no. 4, pp. 1190–1199, Oct. 2015.

[15] L. W. J. Juang, X. Yan, M. Sikaria, R. Zhao, P. J. Weicker, and A. Paryani, "Electric vehicle battery monitoring system," U.S. Patent 10,183,590, Jan. 22, 2019.

[16] A. A. Hussein and A. A. Chehade, "Robust artificial neural network-based models for accurate surface temperature estimation of batteries," *IEEE Trans. Ind. Appl.*, vol. 56, no. 5, pp. 5269–5278, Sep./Oct. 2020.

[17] F. Feng et al., "Co-estimation of lithium-ion battery state of charge and state of temperature based on a hybrid electrochemical-thermal-neural-network model," *J. Power Sources*, vol. 455, 2020, Art. no. 227935.

[18] M. Naguib, P. Kollmeyer, and A. Emadi, "Application of deep neural networks for lithium-ion battery surface temperature estimation under driving and fast charge conditions," *IEEE Trans. Transp. Electrific.*, early access, 2022, doi: 10.1109/TTE.2022.3200225.

[19] M. M. Hasan, S. A. Pourmousavi, A. J. Ardakani, and T. K. Saha, "A data-driven approach to estimate battery cell temperature using a nonlinear autoregressive exogenous neural network model," *J. Energy Storage*, vol. 32, 2020, Art. no. 101879.

[20] Y. Jiang, Y. Yu, J. Huang, W. Cai, and J. Marco, "Li-ion battery temperature estimation based on recurrent neural networks," *Sci. China Technological Sci.*, vol. 64, no. 6, pp. 1335–1344, 2021.

[21] M. Sajid, A. Wadi, M. Abdel-Hafez, and A. A. Hussein, "An extended Kalman filter with exponential thermoelectric measurement model for sensorless surface temperature estimation of Li-ion batteries," in *Proc. IEEE Energy Convers. Congr. Expo.*, 2021, pp. 5903–5906.

[22] A. Wadi, M. F. Abdel-Hafez, and A. A. Hussein, "Mitigating the effect of noise uncertainty on the online state-of-charge estimation of Li-ion battery cells," *IEEE Trans. Veh. Technol.*, vol. 68, no. 9, pp. 8593–8600, Sep. 2019.

[23] B. Gao, S. Gao, G. Hu, Y. Zhong, and C. Gu, "Maximum likelihood principle and moving horizon estimation based adaptive unscented Kalman filter," *Aerosp. Sci. Technol.*, vol. 73, pp. 184–196, Feb. 2018.

[24] B. J. Odelson, M. R. Rajamani, and J. B. Rawlings, "A new autocovariance least-squares method for estimating noise covariances," *Automatica*, vol. 42, no. 2, pp. 303–308, Feb. 2006.

[25] M. R. Rajamani and J. B. Rawlings, "Estimation of the disturbance structure from data using semidefinite programming and optimal weighting," *Automatica*, vol. 45, no. 1, pp. 142–148, Jan. 2009.

[26] M. A. Zagrobelny and J. B. Rawlings, "Identifying the uncertainty structure using maximum likelihood estimation," in *Proc. Amer. Control Conf.*, 2015, pp. 422–427.

[27] M. S. El Din, M. F. Abdel-Hafez, and A. A. Hussein, "Enhancement in Li-ion battery cell state-of-charge estimation under uncertain model statistics," *IEEE Trans. Veh. Technol.*, vol. 65, no. 6, pp. 4608–4618, Jun. 2016.

[28] C. Birkl, *Oxford Battery Degradation Dataset 1*. New York, NY, USA: Oxford, 2017.

[29] "NASA public battery ageing dataset," Accessed: Nov. 20, 2022. [Online]. Available: https://data.nasa.gov/dataset/Li-ion-Battery-Aging-Datasets/uj5r-zjdb
[30] I. Rhee, M. F. Abdel-Hafez, and J. L. Speyer, "Observability of an integrated GPS/INS during maneuvers," *IEEE Trans. Aerosp. Electron. Syst.*, vol. 40, no. 2, pp. 526–535, Apr. 2004.
[31] W. M. F. Al-Masri, M. F. Abdel-Hafez, and M. A. Jaradat, "Inertial navigation system of pipeline inspection gauge," *IEEE Trans. Control Syst. Technol.*, vol. 28, no. 2, pp. 609–616, Mar. 2020.
[32] L. Patnaik, A. V. Praneeth, and S. S. Williamson, "A closed-loop constant-temperature constant-voltage charging technique to reduce charge time of lithium-ion batteries," *IEEE Trans. Ind. Electron.*, vol. 66, no. 2, pp. 1059–1067, Feb. 2018.
[33] A. M. Elsergany, A. A. Hussein, A. Wadi, and M. F. Abdel-Hafez, "An adaptive autotuned polynomial-based extended Kalman filter for sensorless surface temperature estimation of Li-ion battery cells," *IEEE Access*, vol. 10, pp. 14038–14048, 2022, doi: 10.1109/ACCESS.2022.3148281.

Mahroo Sajid received the B.S. degree in electrical engineering from the College of Electrical and Mechanical Engineering, Rawalpindi, Pakistan, in 2009. She is currently working toward the M.S. degree in mechatronics engineering with the American University of Sharjah, Sharjah, UAE.

Her research interests include swarm robotics, self-organization, estimation theory, and robotic control systems.

Ala A. Hussein (Senior Member, IEEE) received the B.S. degree from Jordan University of Science and Technology, Irbid, Jordan, in 2005, and the M.S. and Ph.D. degrees from the University of Central Florida, Orlando, FL, USA, in 2008 and 2011, respectively, all in electrical engineering.

He is an Associate Professor with the Department of Electrical Engineering, Prince Mohammad Bin Fahd University, Khobar, Saudi Arabia. He also holds a joint appointment with the Florida Solar Energy Center, University of Central Florida. He has authored or coauthored more than 70 papers in refereed journals and conference proceedings.

Dr. Hussein has been awarded multiple Research Excellence awards, successfully competed for a number of research grants totaling around $0.4 M. He was listed in Stanford University's top 2% most-cited scientists worldwide in the field of Electrical and Electronic Engineering (subfield of Energy) in 2019, 2020, and 2021.

Ali Wadi (Member, IEEE) received the B.Sc. (*cum laude*) and M.Sc. degrees in mechanical engineering from the American University of Sharjah, Sharjah, UAE, in 2015 and 2017, respectively.

He is currently a Laboratory Instructor with the Department of Mechanical Engineering, American University of Sharjah. He has authored or coauthored more than 20 papers in leading refereed journals and conference proceedings. His research interests include robotics, modeling, nonlinear dynamics, control systems, drug delivery systems, stochastic estimation, and sensor fusion.

Mamoun F. Abdel-Hafez (Senior Member, IEEE) received the B.S. degree from the Jordan University of Science and Technology, Irbid, Jordan, in 1997, the M.S. degree from the University of Wisconsin, Milwaukee, WI, USA, in 1999, and the Ph.D. degree from the University of California at Los Angeles (UCLA), Los Angeles, CA, USA, in 2003, all in mechanical engineering.

In 2003, he served as a Postdoctoral Research Associate with the Department of Mechanical and Aerospace Engineering, UCLA, where he was involved in a research project on fault-tolerant autonomous multiple aircraft landing. He is currently a Professor with the Department of Mechanical Engineering, American University of Sharjah, Sharjah, UAE. His research interests include stochastic estimation, control systems, sensor fusion, and fault detection.